Available online at www.sciencedirect.com

SciVerse ScienceDirect

Ceramics International 39 (2013) 8319–8326

CERAMICS INTERNATIONAL

www.elsevier.com/locate/ceramint

Photoluminescence properties of Ca–α-SiAlON:Ce^{3+} phosphors as function of composition and microstructure

Lin Gan[a,b], Zhi-Yong Mao[b,c], Yi-Fei Wang[d], Fang-Fang Xu[a,*], Ying-Chun Zhu[c], Qing Huang[d], Xue-Jian Liu[e]

[a]State Key Laboratory of High Performance Ceramics and Superfine Microstructures, Shanghai Institute of Ceramics, Chinese Academy of Sciences, Shanghai, 200050, PR China

[b]University of Chinese Academy of Sciences, Beijing 100049, PR China

[c]Inorganic Coating Materials Research Center, Shanghai Institute of Ceramics, Chinese Academy of Sciences, Shanghai, 200050, PR China

[d]Division of Functional Materials and Nanodevices, Ningbo Institute of Materials Technology and Engineering, Chinese Academy of Sciences, Ningbo 315210, PR China

[e]The Research Center of Structural Ceramic Engineering, Shanghai Institute of Ceramics, Chinese Academy of Sciences, Shanghai, 200050, PR China

Received 15 February 2013; received in revised form 22 March 2013; accepted 22 March 2013
Available online 10 April 2013

Abstract

Cerium-doped Ca–α-SiAlON phosphors with $Ca_{n-1.5x}Si_{12-m-n}Al_{m+n}O_nN_{16-n}:Ce_x$ ($m=2n$, $0.8\leq m\leq 2.4$, and $0.02\leq x\leq 0.40$) nominal compositions have been synthesized by gas pressure sintering (GPS). The photoluminescence (PL) properties were studied in relation to phase composition, particle morphology, and microstructure. Continuous addition of Ce rare-earth (RE) could enhance the emission intensity of phosphors, which was partially attributed to the formation of increased amount of planar defects where dense doping of Ce ions is achieved. Such enhancement could hold up to $x=0.32$, above which the emission intensity fell slightly due to the formation of more secondary phases and a surface glassy phase rather than concentration quenching. Finally, possible ways to improve the luminescence properties of Ce-doped α-SiAlON phosphors were discussed through tailoring the composition and microstructure.

Keywords: D. SiAlON; Luminescence; Composition; Microstructure

1. Introduction

α-SiAlON is a solid solution isostructural with α-Si_3N_4 and is stabilized by the interstitial dissolution of a cation (M) of Li, Ca, Mg, Y or some lanthanides [1]. Its general formula can be given as $M_xSi_{12-m-n}Al_{m+n}O_nN_{16-n}$ ($x=m/v$, v is the valence of metal M) [2]. In the α-SiAlON structure, $m+n$ Si–N bonds are replaced by m Al–N and n Al–O bonds. Therefore, M^{v+} cations must be introduced into the large interstices of the α-SiAlON lattice for charge balance. α-SiAlON is known as a promising engineering ceramic material and has been used in numerous important applications due to its superior mechanical properties, chemical inertness and thermal shock resistance [3]. In recent years, α-SiAlON has also been discovered as an excellent host material for RE-doped phosphors showing high luminescence efficiency comparable to commercial yttrium–aluminum-garnet (YAG:Ce) and silicate phosphors. A series of intense research on α-SiAlON:RE (RE=Eu^{2+}, Ce^{3+}, Sm^{3+}, Dy^{3+}, Tb^{3+}, Pr^{3+} and Yb^{2+}) has been carried out focusing on their optical properties [3–11]. One of the most attractive advantages of RE-doped α-SiAlON phosphors over conventional oxide, sulfide and halide phosphors are their high thermal quenching resistance, which resulted from the strong covalent bonds of (Si, Al)–(N, O) [5,12].

Among those RE elements used in α-SiAlON phosphors, Eu and Ce are the two that have attracted most research interest owing to their showing strong luminescence of yellow-orange and blue-green lights, respectively. Compared to extensive studies available with respect to α-SiAlON:Eu phosphors,

*Corresponding author. Tel.: +86 21 52412574; fax: +86 21 52415615.
E-mail address: ffxu@mail.sic.ac.cn (F.-F. Xu).

0272-8842/$ - see front matter © 2013 Elsevier Ltd and Techna Group S.r.l. All rights reserved.
http://dx.doi.org/10.1016/j.ceramint.2013.03.102

researches on α-SiAlON:Ce phosphors are still not systematic. van Krevel et al. were the first that discovered interesting luminescence properties of Ce-doped Y–α-SiAlON [13]. Later, Xie et al. briefly reported PL of Ce-doped Y–α-SiAlON and Ca–α-SiAlON [3,6]. Very recently, Li et al. studied the optical properties of Ce and Li co-doped Ca–α-SiAlON, showing influence of m and n values and doping concentration on the luminescence [7]. Ce-doped α-SiAlON exhibits interesting microstructure, which makes it to be distinguished from other RE-doped α-SiAlON materials. Esktröm et al. revealed a specific type of defect and suggested that it should be related to the non-uniform distribution of cerium ions in the α-SiAlON lattice [14]. Our previous and recent work has confirmed the congregation of Ce ions within these structural defects, i.e. faults formed via a translation of 1/3⟨210⟩-type along with an inversion operation [2,15,16]. Meanwhile, micro-analysis of luminescence properties via using a cathodoluminescence (CL) spectrometer attached to a scanning electron microscope (SEM) revealed that these faults with proper shapes might give rise to enhanced luminescence intensity [17].

Apparently, the specific microstructure of α-SiAlON:Ce phosphors should have a certain effect on the luminescence properties. Therefore, in this work, we aim to investigate the luminescence properties of Ca–α-SiAlON:Ce phosphors through tailoring the microstructure by adjusting the matrix composition and Ce concentration. It will be seen that there exists a close relationship among luminescence, phase composition, and microstructure.

2. Experimental procedures

A group of Ce-doped Ca–α-SiAlON phosphors with nominal compositions of $Ca_{n-1.5x}Si_{12-m-n}Al_{m+n}O_nN_{16-n}:Ce_x$ ($m=2n$, $0.8\leq m\leq 2.4$, $0.02\leq x\leq 0.40$) were synthesized from α-Si_3N_4 (SN-E10, Ube Industries, Japan), AlN (Type F, Tokuyama Corp., Japan), $CaCO_3$ (99.99%, Aladdin, China) and CeO_2 (99.99%, Aladdin, China) powders. The raw powders were mixed homogeneously in an agate mortar. Subsequently, the powder mixture was loaded into boron nitride crucibles and fired in a GPS furnace at 1700 °C for 2 h under a N_2 gas pressure of 0.6 MPa. After firing, the samples were cooled down naturally to room temperature in the furnace. The fired samples were ground in the agate mortar for further characterization.

Phase identification of the synthesized powders was performed by X-ray diffraction (XRD, AXS D8 Focus, Bruker, Germany) analysis using Cu Kα radiation ($\lambda=1.5406$ Å) at 40 kV and 40 mA with a graphite monochromator. A step size of 0.02° was used with a scan speed of 6 deg/min. The morphology of phosphor particles was observed using a SEM (JEM-6390, JEOL, Japan). The PL spectra were measured by a fluorescence spectrophotometer (FluoroMax-4, Horiba, Japan) at room temperature. Microstructure analysis was performed using a 200 kV field-emission transmission electron microscope (TEM, JEM-2100F, JEOL, Japan) equipped with an energy dispersive spectrometer (EDS, INCA Energy, Oxford Instruments, UK).

3. Results and discussion

Fig. 1(a) shows the XRD patterns of samples with various m values ($m=2n$, $0.8\leq m\leq 2.4$) and a fixed $x=0.02$, i.e. an identical Ce addition while different amounts of Al and O substitution. At $m=0.8$, trace amount of β-SiAlON phase is identified besides the dominant α-SiAlON phase. Upon increasing the m value, single α-SiAlON phase is obtained. Additionally, the inset shows that the diffraction peaks of α-SiAlON gradually shift to low diffraction angles with the increase of m value, indicating a continuous expansion of the crystal lattice. The increase of lattice parameters is attributed to the growing number of shorter Si–N bonds (1.74 Å) replaced by longer Al–N bonds (1.87 Å) and Al–O bonds (1.75 Å), which coincides with the increasing m value. Fig. 1(b) gives the XRD spectra of samples with various x values ($0.02\leq x\leq 0.40$) and a fixed $m=2.0$, showing the effect of Ce addition on the phase structure. Phase pure α-SiAlON is obtained when $x\leq 0.16$, while minor impurity phases are detected in the samples with $x\geq 0.24$. Small amount of AlN

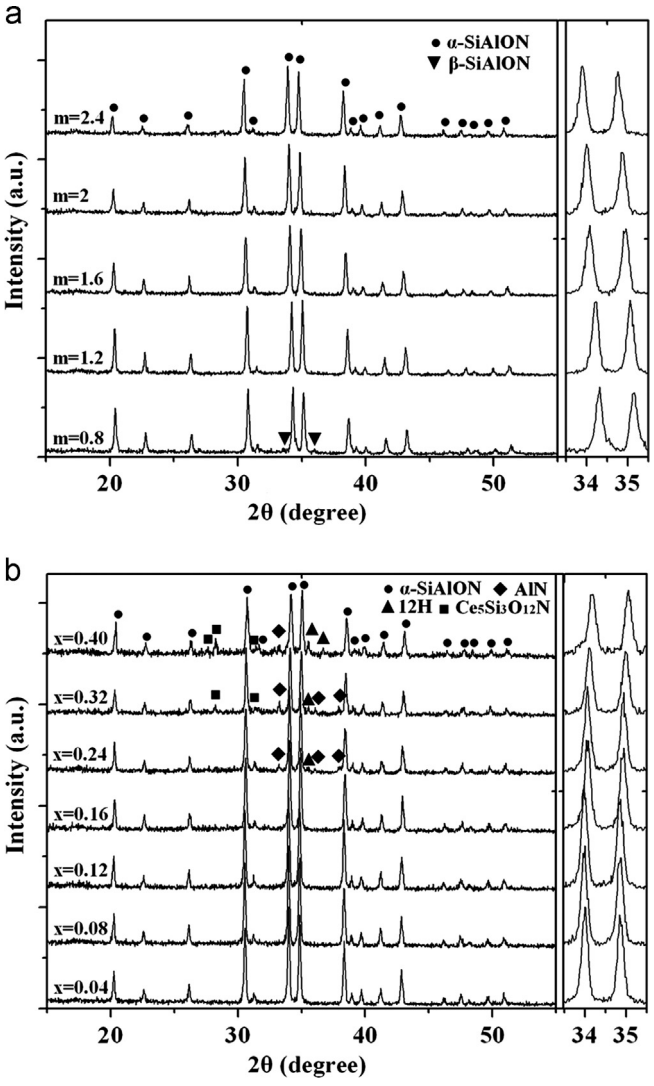

Fig. 1. XRD patterns of the synthesized Ce^{3+}-doped Ca–α-SiAlON phosphors at (a) $x=0.02$ with various m values and (b) $m=2.0$ with various x values.

and AlN polytypoid phase (12H) appear in the samples with $x=0.24$. At higher x values ($x=0.32$ and 0.40), cerium-rich $Ce_5Si_3O_{12}N$ phase is also observed besides AlN and 12H phases. It is known that Ce^{3+} ions cannot stabilize the α-SiAlON structure alone but can enter the lattice with the simultaneous incorporation of a smaller stabilizing metal cation, such as Y^{3+} or Ca^{2+} [1,6,18]. However, the solubility of Ce in the α-SiAlON grain is much lower than that of Y, Mg and Ca [14,16]. Therefore, in the samples synthesized with higher amount of CeO_2 in the starting powders, some Ce ions failed to enter the α-SiAlON lattice, resulting in the formation of Ce-rich impurity phase. The inset of Fig. 1(b) does not show obvious shift of diffraction peaks until the x value increases to 0.16, from which the peak location shifts to a high diffraction angle, suggesting a continuous shrinkage of the α-SiAlON lattice. This lattice shrinkage, as will be discussed later, is associated with the influence of x value on the actual composition of the α-SiAlON phase.

SEM images of the samples with varying m values ($m=0.8$, 2.0, and 2.4; $x=0.02$) and x values ($x=0.04$, 0.08, and 0.24; $m=2$) are presented in Fig. 2(a–c) and Fig. 2(d–f), respectively. When x value is fixed, increasing of m value simply gives rise to coarsening of grains with an equiaxed shape. Nevertheless, the particles tend to be irregular rather than prismatic shaped and large agglomerates form when m reaches to 2.4. Grain coarsening with increasing m values could be attributed to the increased amount of transient liquid phase that accelerates the dissolution, diffusion and precipitation processes during grain growth. Similarly, increasing of x value at a fixed $m=2.0$ also results in the increase of particle size (see Fig. 2(b,d–f)) along with agglomeration of particles. CeO_2 is an efficient sintering additive of SiAlON materials. Upon increasing CeO_2 addition, the increased transient liquid phase accelerates the grain growth as well as sintering of the sample.

Fig. 3 shows the PL spectra of Ce^{3+}-doped Ca–α-SiAlON phosphors under excitation at 375 nm and monitored at 485 nm. The emission spectra exhibit a single emission band peaked near 480 nm. Such emission should be attributed to the $4f^05d^1 \rightarrow 4f^1$ transition of Ce^{3+} ions. It is clearly seen in Fig. 3 that both host composition (m value) and Ce concentration (related to x value) affect the light emission of Ce^{3+}-doped Ca–α-SiAlON phosphors. The emission intensity increases with increasing of m value from 0.8 to 2 and then decreases. As observed by SEM, the sample with $m=0.8$ has the smallest

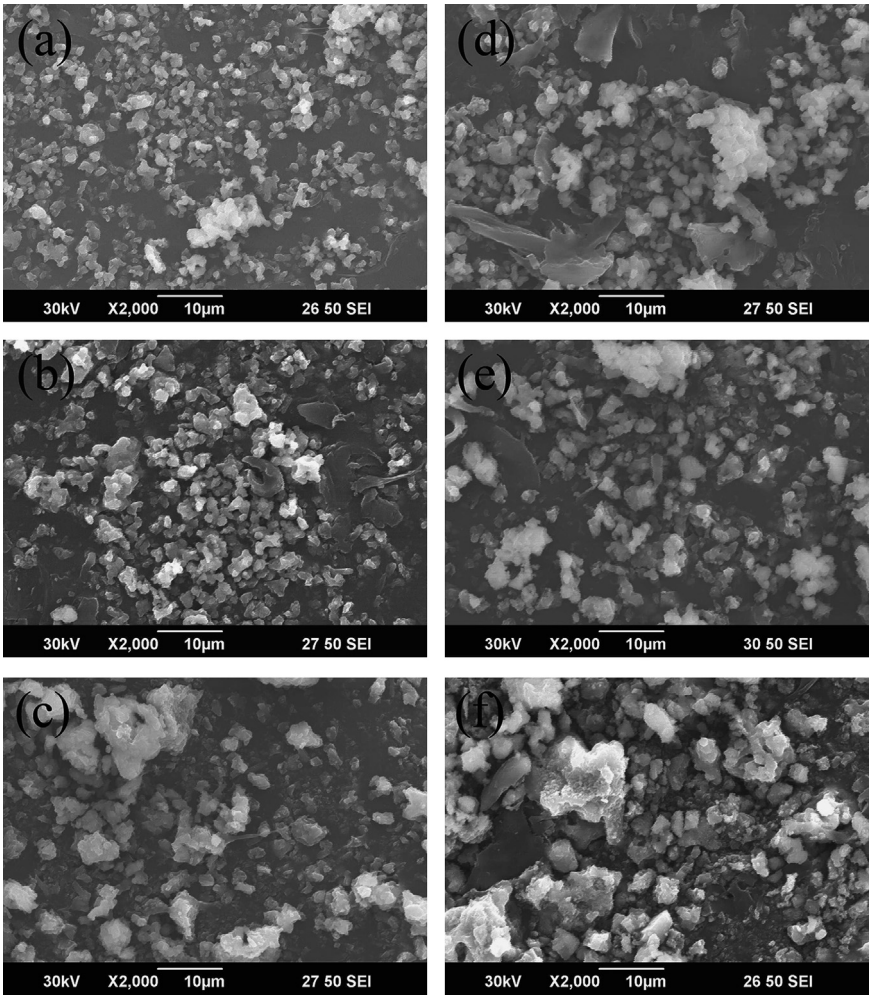

Fig. 2. SEM images of Ce^{3+}-doped Ca–α-SiAlON phosphors. (a), (b) and (c) with m values of 0.8, 2.0 and 2.4 respectively, while the x value is fixed at 0.02; (d), (e) and (f) with x values of 0.04, 0.08 and 0.24 respectively, while the m value is fixed at 2.0.

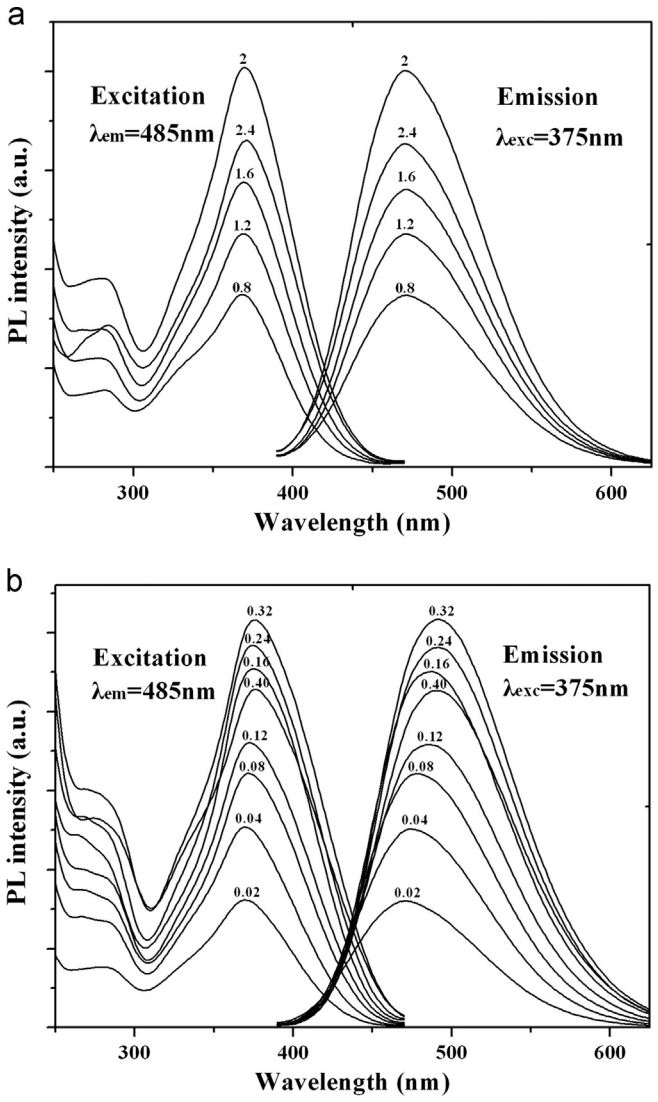

Fig. 3. Excitation and emission spectra of Ce^{3+}-doped Ca–α-SiAlON phosphors. (a) $x=0.02$ with various m values; (b) $m=2.0$ with various x values ($\lambda_e m=485$ nm and $\lambda_{exc}=375$ nm for each sample).

grain size, indicating poor crystallinity due to a smaller amount of transient liquid phase. Therefore, defects in the grains could trap or scatter the emitting light and eventually reduce the emission intensity [3]. Meanwhile, the β-SiAlON impurity phase detected by XRD could also take negative effect. For the sample with $m=2.4$, deterioration of luminescence should be attributed to the large agglomerates of α-SiAlON grains, which leads to a relatively low packing density in the measurement and hence a strong light scattering. The emission peak presents a continuous shift toward long wave side from 470 nm ($m=0.8$) to 473 nm ($m=2.4$) with increasing of m value. The red shift phenomenon was also reported in other RE-doped α-SiAlON materials [5]. Increase in the m value indicates larger number of shorter and stronger Si–N bonds replaced by longer and weaker Al–N bonds, hence less rigidity of the α-SiAlON lattice. As a result, the Stokes shift becomes larger upon increasing the m value, which leads to the red shift of the emission wavelength. Nevertheless, the change of m value shows little influence on the location of the excitation peak.

Variety of Ce addition also shows considerable influence on the luminescence as could be seen in Fig. 3(b) for the samples with a fixed $m=2$ and different x values. A red shift in the excitation and emission spectra can be observed when the x value increases from 0.02 to 0.40. The main excitation band shifts from 370 to 376 nm and the corresponding emission band shifts from 472 to 492 nm. It is worth to note that the red shift of the emission band stops at 492 nm for $x=0.24$, while further increase in the x value would not cause obvious band shift. The lattice shrinkage revealed by XRD (see the inset of Fig. 1(b)) probably takes certain effect against the increased Ce doping concentration and stops the red shift due to the reduced Stokes shift. The red shift of emission wavelength could be mainly caused by the reabsorption process. In Fig. 3, the excitation and emission spectra show overlapping at 400–460 nm. Therefore, with increasing Ce concentration, the reabsorption between Ce^{3+} ions becomes stronger and reduces the emission of the short wave wing, resulting in the upward shift of the emission band. The PL intensity rises continuously with the x value increasing up to 0.32, and then falls at even higher x value. The decrease of emission intensity at the highest x value should arise from the increased amount of impurity phases and severe agglomeration of the particles. Then, compared to other RE-doped α-SiAlONs which show concentration quenching at much lower x values (i.e. 0.075, 0.07, 0.05 and 0.005 for Eu, Sm, Tb and Yb, respectively) [3,5,11], much more Ce ions seem to be able to enter the α-SiAlON lattice without considerable decay in luminescence intensity. In fact, we observed in our recent work strong emission at fault sites where the theoretically maximum doping concentration of Ce ions was achieved, i.e. each interstice is occupied by a Ce ion at faults [17]. No concentration quenching seems to occur for the Ce–α-SiAlON system though structural defects, impurity phases and agglomerates would attenuate the luminescence intensity.

In order to clarify the actual composition of as-obtained phosphors and the role of microstructure in factors affecting the luminescence properties, we performed detailed analyses by TEM-EDS. Fig. 4(a) is the TEM image of an α-SiAlON grain in the sample with $m=2$ and $x=0.02$. Its magnified image (Fig. 4(b)) clearly shows the fault contrast. The high-resolution electron microscopy (HREM) image and the electron diffraction pattern (Fig. 4(c)) indicate the two intersectional faults located on the (001) and (011) plane, respectively. These particular faults in Ce–α-SiAlON have been identified to be formed via a 1/3⟨210⟩-type lattice displacement along with an inversion operation [16]. Faults in Ce–α-SiAlON have been proved to be directly related to the dense doping of Ce in these defect sites. In this sample, only very few grains contain faults and the fault density is quite low apparently because of the low Ce doping concentration. Actually, it will be seen later that fault density increases with x value. In Fig. 4(d), a layer (about 20 nm) of amorphous phase is observed on the surface of the grain. In fact, glassy layer can be found in almost every grain of every sample in the present work. EDS analysis indicates

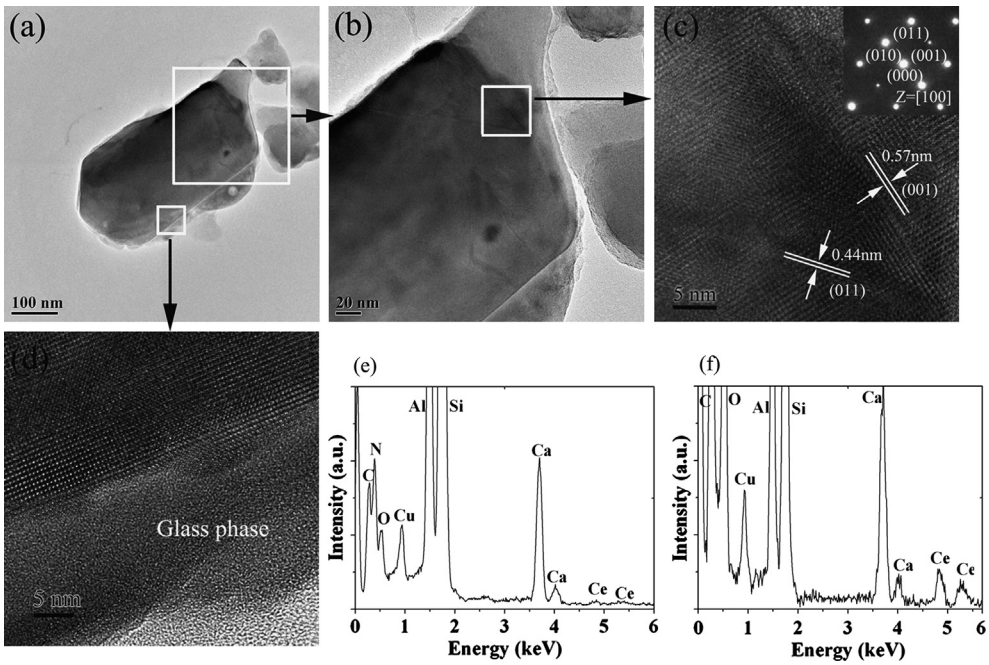

Fig. 4. TEM micrographs and EDS spectra of the sample with $m=2$ and $x=0.02$. (a) TEM image of an α-grain; (b) the magnified image of the large framed region in (a) showing faults in the grain; (c) [100]-projected HREM image of the faults and the corresponding diffraction pattern in the inset; (d) HREM image showing glassy phase on the grain surface; (e) and (f) EDS spectra obtained from the α-SiAlON grain and the surface glassy phase, respectively (Cu and C peaks came from copper grid and carbon-coated supporting film, respectively).

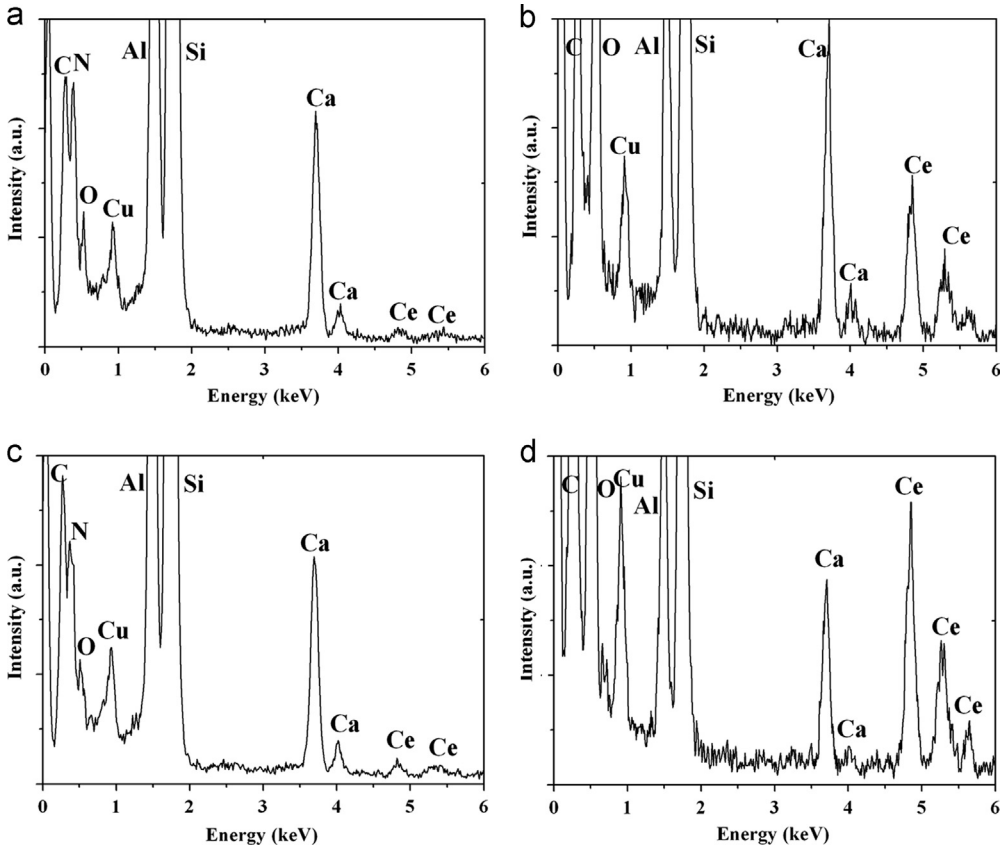

Fig. 5. EDS spectra obtained from the α-SiAlON grain and the surface glassy phase, (a) and (b) for the sample with $m=2$, $x=0.04$; (c) and (d) for the sample with $m=2$, $x=0.08$.

that very small amount of Ce ions has been incorporated into the α-SiAlON structure (Fig. 4(e)) whereas Ce ions are abundant in the oxygen-rich surface glassy phase (Fig. 4(f)). This suggests that considerable amount of Ce ions failed to enter the α-SiAlON lattice while they remained in the surface amorphous phase. It is widely believed that the formation of oxygen-rich surface and intergranular glassy phase is inevitable in SiAlON materials synthesized by liquid-phase kinetics where oxide impurities covering the nitride raw powders along with the RE oxides form transient liquid phase during the firing process. RE elements such as Ce, Yb, Sm and Dy are more apt to stay in the oxygen-rich glassy phase than to enter the α-SiAlON lattice [18,19].

Fig. 5(a–d) are the EDS spectra obtained from the α-SiAlON grain and the surface glassy phase of the samples with $x=0.04$ (Fig. 5(a) and (b)) and $x=0.08$ (Fig. 5(c) and (d)). Compared to the sample with $x=0.02$ (see Fig. 4(e) and (f)), the Ce content in the α-SiAlON lattice increases very slightly with the increase of Ce addition (x value) from 0.02 to 0.08 in the nominal composition, whereas dramatic increase of the Ce concentration is identified in the surface glassy phase. Therefore, a simple increment of Ce components in the raw materials does not seem to necessarily trigger more Ce ions into the α-SiAlON lattice. However, as will be seen below, more addition of Ce in the raw materials will lead to the formation of higher density of faults, suggesting actually higher amount of Ce entering the host lattice though the distribution is uneven.

When more Ce ions try to enter the α-SiAlON structure, they congregate into the faults rather than evenly distribute in the crystal lattice. Meanwhile, the structure of faults changes from individual wide planar shapes to narrow facets on some specific crystallographic planes which intersect to form domains. Moreover, the size of domains decreases while their density increases upon increasing x values (see Fig. 6). Formation of the faults or domain boundaries is a typical structural feature in Ce-doped α-SiAlON crystals even at a low Ce doping ($x=0.02$, see Fig. 4). Such faults have never been observed in α-SiAlON materials doped with other RE ions. Additionally, different synthesis methods (e.g. hot isostatic pressing or spark plasma sintering) or multi-doping (e.g. with Y and Ca) do not show much difference in the formation of faults [1,14].

In view of the above analysis results, it is necessary to investigate the actual chemical composition of the Ce^{3+}-doped Ca–α-SiAlON crystallites with various x values. Thus EDS quantification in TEM was employed to the samples with x=0.16, 0.24, 0.32 and 0.40. In order to exclude the influence of surface glassy layer on the composition analysis, all the

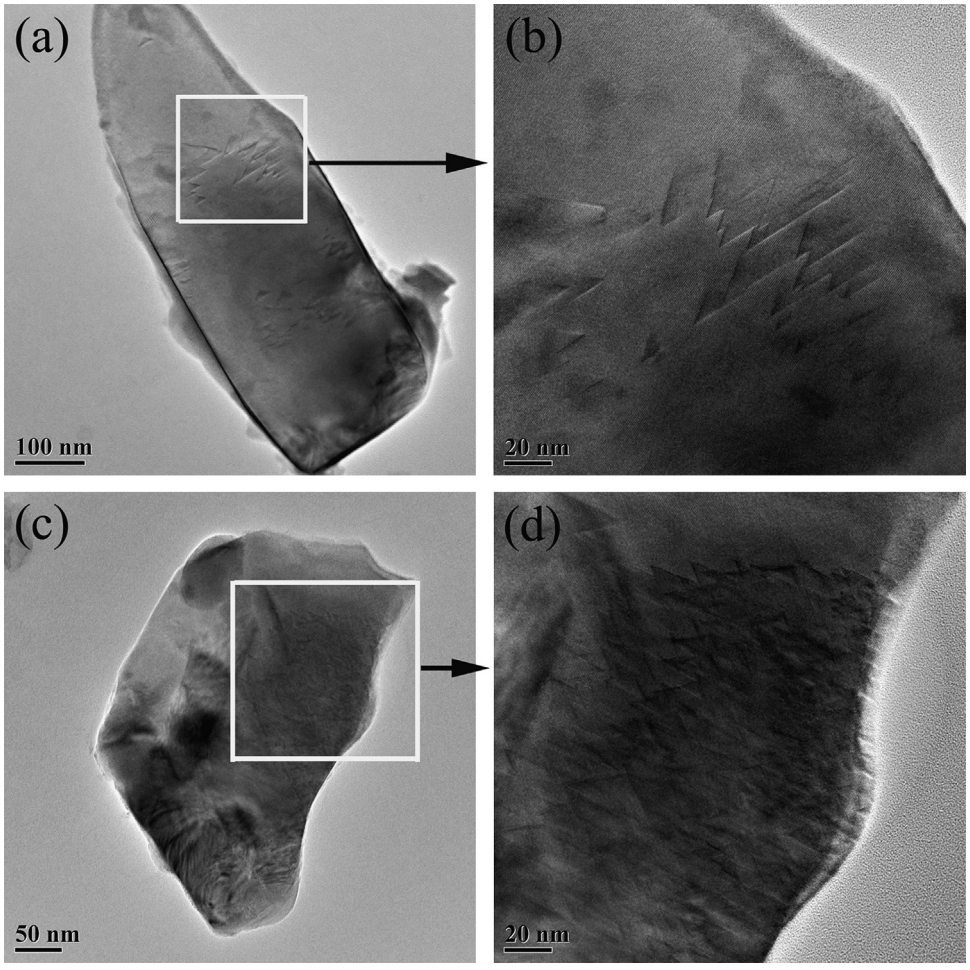

Fig. 6. TEM micrographs of the α-SiAlON grain in the samples with $x=0.24$ (a, b) and $x=0.40$ (c, d) at a fixed $m=2$.

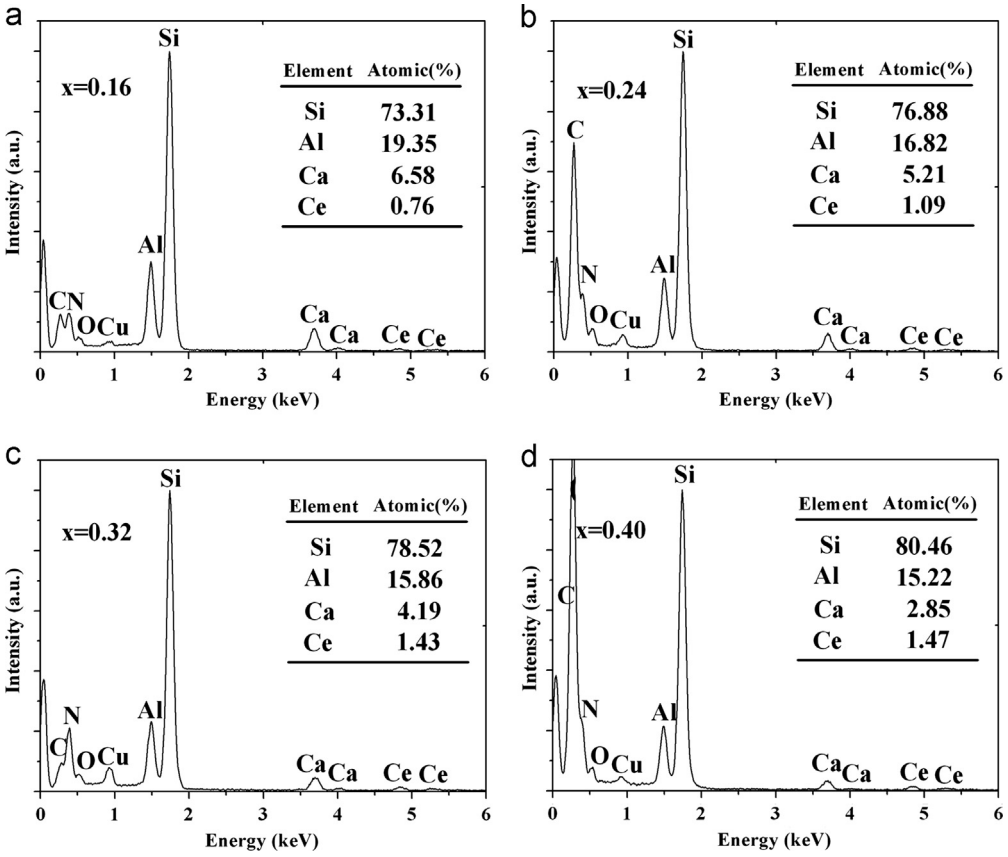

Fig. 7. EDS spectra and corresponding quantification results from α-SiAlON grains in the samples with various x values.

samples for following EDS examination were ground repeatedly and then soaked in 5 wt% HF solution for 1 h to remove the surface amorphous phase. Here for critical charge balance, we give the Ce^{3+}-doped Ca–α-SiAlON a general formula $Ca_{m'/2}Ce_{m''/3}Si_{12-m-n}Al_{m+n}O_nN_{16-n}$, where m is the number of Si–N bonds replaced by Al–O, n the number of Si–N bonds replaced by Al–N, the numbers 2 and 3 refer to the valence of Ca and Ce, respectively, and $m'+m''=m$. It should be noted here that the m value in this formula is not the nominal but the actual m obtained by the EDS quantification.

Fig. 7 gives the results of the EDS quantitative analysis, in which N and O are not taken into account because of the interference of the C peak close to them as well as the large error in EDS quantification for light elements such as N and O. All the data were obtained in the matrix lattice of Ce–Ca–α-SiAlON while faulted area and glassy phase were avoided. It should be seen that each element shows a certain regular change in the content with increasing x value, i.e. Si and Ce rise while Al and Ca drop in concentration. This indicates that the actual $m+n$ value in α-SiAlON decreases with the increasing x value. The occurrence of residual AlN identified by XRD (see Fig. 1(b)) in the samples with $x \geq 0.24$ coincides with the reduced Al content in the α-SiAlON phase. The EDS results indicate the decrease of overall metal incorporation and increase of Ce/Ca doping ratio with the increment of x value from 0.16 to 0.40. The general formula indicates that $m'/2$ and $m''/3$ are directly proportional to the Ca and Ce concentrations in α-SiAlON, respectively. From Fig. 7 we can find that the actual m value, which is proportional to 2Ca%+3Ce%, decreases with increasing x value (i.e. 2Ca%+3Ce% = 15.44, 13.69, 12.67 and 10.11 (%) for $x=0.16$, 0.24, 0.32 and 0.40 respectively). Large ions such as Ce^{3+} and Eu^{2+} are not as easy as smaller ones (e.g. Ca^{2+} and Y^{3+}) to be accommodated into the interstices of α-SiAlON structure. The EDS results (see Figs. 4 and 5) confirmed that a considerable proportion of Ce ions actually segregated in the glassy phase rather than entering the α-SiAlON structure at higher x values. Decrease of the actual m value leads to the lattice shrinkage of the α-SiAlON phase, which is proved by the shift of XRD peaks toward high diffraction angles (see the inset of Fig. 1(b)). Although the variation of actual n value cannot be clearly identified, its influence on the lattice parameters of α-SiAlON is negligible [7]. This is because Al–N bonds (1.87 Å) have much greater discrepancy in bond length with respect to Si–N bonds (1.74 Å) than Al–O bonds (1.75 Å), hence a greater effect of m value on the lattice parameters than n value. The actual Ce doping concentration (actual x value) in the matrix lattice of the four samples can be calculated to be 0.098, 0.140, 0.182 and 0.184 for $x=0.16$, 0.24, 0.32 and 0.40 in their nominal composition, respectively. It should be emphasized here that these calculated results must be lower than the overall Ce concentration in the α-SiAlON grains containing faults where the highest doping of Ce is achieved.

The phosphors applied to white light-emitting diodes (LEDs) must have high phase purity, uniform particle size and high luminescence intensity. The present work clearly shows that higher Ce doping concentration gives rise to stronger PL emission of the Ce^{3+}-doped Ca–α-SiAlON phosphors. However, the simultaneous formation of impurity phases and severe agglomeration of the particles should be avoided. Meanwhile, the optimal chemical composition and synthesis process, which can both promote the incorporation of Ce into the α-SiAlON structure and reduce the Ce segregation in the surface glass, need further study. Although high *m* value can guarantee good crystallinity, lower *m* value with higher Ce doping concentration (e.g. $x \geq 0.16$) shows greater potential to enhance the luminescence properties. Introduction of more Ce in the starting powder results in the formation of higher density of planar defects where Ce ions congregate and show strong emission of light [17]. Concentration quenching seems to be unavailable for Ce-doped α-SiAlON. Therefore, the coming work should focus on how to optimize the synthesis processes to control the microstructure (i.e. the density and shape of planar defects) and simultaneously avoid or reduce the surface glassy phase, secondary phases and agglomeration of particles.

4. Conclusions

Green-blue emitting Ce-doped Ca–α-SiAlON phosphors have been synthesized by solid-state reaction at 1700 °C. Increasing of either *m* value or Ce doping concentration alone can either improve the crystallinity of phosphor particles or effective incorporation of Ce ions into the host lattice, hence up-grade the luminescence properties. TEM observation shows the dramatically increased density of planar defects with the enhanced Ce incorporation into the α-SiAlON structure, implying a positive influence of the defects on luminescence. However as proved by XRD and EDS analyses, extremely high addition of CeO_2 would lead to the formation of Ce-rich secondary phase or surface glassy phase, which caused deviation of the actual composition of α-SiAlON phase from the nominal one and shrinkage of lattice parameters of α-SiAlON owing to simultaneously lower amount of Si replaced by Al for charge balance. These features along with particle agglomeration upon increasing *m* value and Ce addition could deteriorate the luminescence properties. Therefore, tailoring of phase composition as well as microstructure should be critically carried out in order to further enhance the luminescence properties of Ce-doped Ca–α-SiAlON phosphors.

Acknowledgments

We acknowledge financial supports from the National Natural Science Foundation of China (Nos. 51272270, 60936001 and 51102265), the National Basic Research Program of China (No. 2009CB939904), the CAS/SAFEA International Partnership Program for Creative Research Teams, and the Key Research Program of the Chinese Academy of Sciences.

References

[1] C.-M. Wang, M. Mimoto, F.-F. Xu, N. Hirosaki, Y. Bando, Synthesis of cerium α-SiAlON with nuclei addition, Journal of the American Ceramic Society 84 (2001) 1389–1391.
[2] F.-F. Xu, Y. Bando, C.-M. Wang, M. Mimoto, Distribution of cerium ions in cerium-doped α′-SiAlON and its effect on grain morphology, Journal of the American Ceramic Society 85 (2002) 466–472.
[3] R-.J. Xie, N. Hirosaki, M. Mimoto, T. Suehiro, X. Xu, H. Tanaka, Photoluminescence of rare-earth-doped Ca–α-SiAlON phosphors: composition and concentration dependence, Journal of the American Ceramic Society 88 (2005) 2883–2888.
[4] R.-J. Xie, N. Hirosaki, K. Sakuma, Y. Yamamoto, M. Mimoto, Eu^{2+}-doped Ca–α-SiAlON: a yellow phosphor for white light-emitting diodes, Applied Physics Letters 84 (2004) 5404–5406.
[5] R.-J. Xie, N. Hirosaki, M. Mimoto, Y. Yamamoto, T. Suehiro, K. Sakuma, Optical properties of Eu^{2+} in α-SiAION, Journal of Physical Chemistry B 108 (2004) 12027–12031.
[6] R.-J. Xie, N. Hirosaki, M. Mimoto, Y. Yamamoto, T. Suehiro, N. Ohashi, Photoluminescence of cerium-doped α-SiAlON materials, Journal of the American Ceramic Society 87 (2004) 1368–1370.
[7] H.-L. Li, G.H. Zhou, R.-J. Xie, N. Hirosaki, X.-J. Wang, Z. Sun, Optical properties of green-blue-emitting Ca–α-Sialon:Ce^{3+},Li^{+} phosphors for white light-emitting diodes (LEDs), Journal of Solid State Chemistry 184 (2011) 1036–1042.
[8] Y.-Q. Li, N. Hirosaki, R.-J. Xie, J. Li, T. Takeda, Y. Yamamoto, M. Mimoto, Structural and photoluminescence properties of Ce^{3+}- and Tb^{3+}-activated Lu–α-Sialon, Journal of the American Ceramic Society 92 (2009) 2738–2744.
[9] R.-J. Xie, M. Mimoto, K. Uheda, F.-F. Xu, Y. Akimune, Preparation and luminescence spectra of calcium and rare-earth (R = Eu, Tb, and Pr)-codoped α-SiAlON Ceramics, Journal of the American Ceramic Society 85 (2002) 1229–1234.
[10] B. Dierre, X.-L. Yuan, N. Hirosaki, R.-J. Xie, T. Sekiguchi, Luminescence properties of Ca- and Yb-codoped SiAlON phosphors, Materials Science and Engineering B 146 (2008) 80–83.
[11] R.-J. Xie, N. Hirosaki, M. Mimoto, K. Uheda, T. Suehiro, X. Xu, Y. Yamamoto, T. Sekiguchi, Strong green emission from α-SiAlON activated by divalent ytterbium under blue light irradiation, Journal of Physical Chemistry B 109 (2005) 9490–9494.
[12] Y.-Q. Zhang, X.-J. Liu, Z.-R. Huang, J. Chen, Y. Yang, PL properties of Eu^{2+}–Mn^{2+} codoped Ca–α-SiAlON phosphors, Journal of Luminescence 132 (2012) 2561–2565.
[13] J.W.H. van Krevel, J.W.T. van Rutten, H. Mandal, H.T. Hintzen, R. Metselaar, Luminescence properties of terbium-, cerium-, or europium-doped α-Sialon materials, Journal of Solid State Chemistry 165 (2002) 19–24.
[14] T. Ekström, K. Jansson, P.O. Olsson, J. Persson, Formation of an Y/Ce-doped α-sialon phase, Journal of European Ceramic Society 8 (1991) 3–9.
[15] F.-F. Xu, Y. Bando, C.-M. Wang, M. Mimoto, Domain-boundary structures in Ce-doped α-(Si–Al–O–N), Philosophical Magazine A 81 (2001) 2271–2284.
[16] F.-F. Xu, E. Sourty, W. Shi, X.-L. Mou, L.-L. Zhang, Direct observation of rare-earth ions in α-Sialon:Ce phosphors, Inorganic Chemistry 50 (2011) 2905–2910.
[17] F.-F. Xu, E. Sourty, X.-H. Zeng, L.-L. Zhang, L. Gan, X.-L. Mou, W. Shi, Y.-C. Zhu, F.-Q. Huang, J.-T. Zhao, Atomic-scaled investigation of structure-dependent luminescence in Sialon:Ce phosphors, Applied Physics Letters 101 (2012) 161904.
[18] E. Söderlund, T. Ekström, Pressureless sintering of Y_2O_3–CeO_2-doped sialons, Journal of Materials Science 25 (1990) 4815–4821.
[19] H. Mandal, D.P. Thompson, T. Ekström, Reversible α→β sialon transformation in heat-treated sialon ceramics, Journal of the European Ceramic Society 12 (1993) 421–429.